EDGE ARTICLE

Check for updates

Janus interface enables reversible Zn-ion battery by regulating interfacial water structure and crystal-orientation†

Yuxuan Liang,‡ Meijia Qiu,‡ Peng Sun* and Wenjie Mai ⓘ *

To tackle the shortcomings of traditional battery systems, there has been much focus on aqueous Zn-ion batteries due to various advantages. However, they still suffer from poor stability of Zn anodes. Here, a methionine additive with unique Janus properties is proposed to regulate the behavior of the interface between Zn anodes and the electrolyte environment. Systematic characterizations as well as calculations elucidate that the Janus additive is adsorbed on the Zn anode *via* zincophilic $-NH_2$, changing the structure of the electric double layer and breaking the hydrogen bonding network among H_2O molecules through hydrophobic $S-CH_3$. At the same time, it can induce preferential formation of $Zn(101)$ with high reversibility. The above two functions contribute to the dendrite inhibiting ability of Zn anodes. As validated, fabricated Zn//Zn symmetric cells achieve stable cycles of 4500 h, 1165 h, and 318 h at 1, 5 and 10 mA cm^{-2}/mA h cm^{-2}, respectively. Furthermore, Zn//Cu asymmetric cells with an average coulombic efficiency of 98.9% for 2200 stable cycles can be realized. Finally, $Zn//MnO_2$ full cells exhibit 79.9% capacity retention with an ultra-high coulombic efficiency of 99.9% for 1000 cycles, much better than that of the pure $Zn(ClO_4)_2$ system, indicating the great potential of this useful strategy in aqueous batteries.

Introduction

Due to the problems of the energy crisis and environmental pollution, the transition from fossil fuel energy to renewable energy is quite essential.[1] However, the unreliability of mainstream renewable energy requires high-performance systems for continuous energy storage. Lithium-ion batteries (LIBs) currently dominate the energy storage market but are still facing the challenges of limited lithium resources, high cost and poor safety issues, which inevitably hinder their further development.[2] Aqueous Zn-ion batteries (AZIBs) are potential alternatives to LIBs due to their abundant reserves, low-cost and theoretically high energy density of Zn anodes. Additionally, the aqueous electrolyte enables their excellent safety and considerable power density.[3] Although promising, there still exist various bottlenecks to overcome before their practical application. Except for the relatively low energy density of the

Siyuan Laboratory, Guangzhou Key Laboratory of Vacuum Coating Technologies and New Energy Materials, Guangdong Key Laboratory of Optical Fiber Sensing and Communications, Guangdong Provincial Key Laboratory of Nanophotonic Manipulation, Guangdong Provincial Engineering Technology Research Center of Vacuum Coating Technologies and New Energy Materials, Department of Physics, Jinan University, Guangdong 510632, People's Republic of China. E-mail: sunp0421@jnu.edu.cn; wenjiemai@email.jnu.edu.cn

† Electronic supplementary information (ESI) available. See DOI: https://doi.org/10.1039/d3sc05334b

‡ These authors contributed equally to this work.

cathodes,[4,5] the poor stability of Zn anodes due to uncontrolled dendrite growth and various side reactions during the reversible plating/stripping process are the main reasons for the degraded performance of AZIBs.[6,7]

To tackle the aforementioned problems, electrode/electrolyte interface (EEI) modification is a feasible way to reduce the uneven deposition of Zn^{2+} on the anode.[8,9] Strategies include constructing artificial interfacial layers on the Zn anode surface,[10–16] altering the solvation structure and improving ion behaviors by electrolyte modifications (such as additive engineering and multi-ion combination).[17–24] Specifically, the mechanisms of the various methods mainly involve adjusting the Zn^{2+} flux,[19,20,22] improving the deposition sites, constructing an electrostatic shielding effect[17,21,25] and regulating the dominant crystal plane.[26–28] Among the above-mentioned methods, it is attractive to design an interfacial component with zincophilic and hydrophobic groups on opposite sides of the Zn anodes, and this has been proved in previous studies.[29–32]

It is well-known that breaking hydrogen bonds is an effective method to reduce free H_2O molecules within the EEI,[33] which can inhibit various side reactions including hydrogen evolution reaction (HER), corrosion, and passivation. Additionally, inducing the formation of the dominant crystal plane, especially $Zn(002)$, is an effective method to achieve uniform deposition on Zn anodes.[28,34] Regarding the relationship between the preferential crystal plane and deposition morphology, we suspect that a uniform deposition morphology can be retained

if a certain crystal plane can be preferentially obtained during reversible plating/stripping processes. Therefore, combining the above two mechanisms through a simple additive strategy to improve the EEI seems to be a feasible strategy to achieve long cycling AZIBs.[35]

Here, we propose a "Janus" additive, methionine (MET), which is hydrophobic on one side and zincophilic on the other side, to inhibit dendrite growth and prevent side reactions by modulating the EEI. Theoretical calculations and experimental results indicate that the MET molecules can adsorb on the Zn anode surface to disrupt the hydrogen bonding (HB) networks among H_2O molecules in the EEI. This reduces the amount of active water on the EEI, greatly inhibiting the HER and related parasitic reactions. It is noteworthy that the MET additive can stably induce the preferential orientation of Zn(101) crystal planes by readjusting the growth rate of different crystal planes. In this modified electrolyte system, the Zn anode has extremely high plating/stripping reversibility as a result of the synergy between the extensive disruption of HB networks from the EEI's water and orientational Zn(101). The fabricated Zn//Zn symmetric cells, Zn//Cu asymmetric cells and Zn//MnO$_2$ full cells, using this optimized electrolyte, all exhibit remarkably improved cycle stability compared with the original electrolyte, which proves that this promising additive engineering strategy can contribute to better performance of future AZIBs.

Results and discussion

Stabilizing function of MET additives for the Zn anode

MET is an essential amino acid for the human body, implying its non-toxic and environmentally-friendly properties. As shown in Fig. 1a, the electrostatic potential distribution (ESP) of the MET molecule indicates that the R group (S–CH$_3$) of MET exhibits low polarity and hydrophobicity. This can enable the effective exclusion of H_2O molecules within the electric double layer (EDL) field of the EEI. In contrast, the ESP around the –NH$_2$ group is the most positive, imparting a zincophilic nature to serve as the potential adsorption and nucleation site of Zn^{2+}. To investigate the practical effect of MET additives in inhibiting dendrite growth, various characterization techniques including scanning electron microscopy (SEM), X-ray diffraction (XRD), and optical microscopy were first conducted. A piece of Zn foil (100 μm) was deposited under different electrolytes with a current density of 10 mA cm^{-2} for 1 h to study the specific effect of the MET additive. To better identify different depositing samples, Zn foils deposited in pure Zn(ClO$_4$)$_2$ and Zn(ClO$_4$)$_2$–MET electrolytes were noted as ND–Zn and MET–Zn, respectively. As illustrated in Fig. 1b, the surface of the ND–Zn shows irregular protrusions, while a regular terraced field morphology is observed on MET–Zn, which can potentially alleviate the dendrite growth process. From the results of electron probe micro analysis (EPMA) in Fig. S1,† the Zn element content of the ND–Zn foil surface was only 70%, which can probably be ascribed to the formation of by-products. In sharp contrast, the MET–Zn surface achieved a much higher Zn element content of around 100%, indicating a highly efficient deposition process.

It should be noted that the XRD patterns demonstrate an increased orientation to Zn(101) on MET–Zn (Fig. 1c), which can be more obviously identified in the 2D figure (Fig. S2†). The intensities of the three main diffraction peaks including Zn(002), Zn(100) and Zn(101) were compared (Fig. S3†). Specifically, the ratio between the intensities ($R_{(101)\text{-rt}} = [I_{(101)}/(I_{(002)} + I_{(100)})]$) of Zn(101) and Zn(002) plus Zn(100) was utilized to analyze the relative variation of Zn(101). As shown in Fig. S3,† the Zn foils deposited in the pure Zn(ClO$_4$)$_2$ electrolyte demonstrated little change in $R_{(101)\text{-rt}}$ (all close to 2), whether under one cycle of deposition or 10 reversible cycles. However, in the Zn(ClO$_4$)$_2$–MET electrolyte, Zn foils exhibited a higher $R_{(101)\text{-rt}}$ (5.29) compared to the original one (2.06), indicating a stronger Zn(101) orientation. Moreover, after 10 plating/stripping cycles, the $R_{(101)\text{-rt}}$ becomes larger (up to 15.38), revealing MET's effective modulating function on the preferential specific crystal plane of Zn(101) during the reversible plating/stripping process of Zn anodes. To further determine the preferential orientation of Zn(101) in the Zn(ClO$_4$)$_2$–MET electrolyte, polar figures with texture information from deposited Zn layer in different electrolyte systems were collected, as presented in Fig. 1d. It can be clearly seen that the Zn(101) pole figure of the Zn foils deposited in the Zn(ClO$_4$)$_2$–MET electrolyte has more enhanced central intensity, as well as weaker and more uniform peripheral intensity, than the sample obtained from the pure Zn(ClO$_4$)$_2$ electrolyte, indicating a predominant Zn(101) crystal-orientation. Calculations were performed to probe the preferential orientation of Zn(101) at the atomic level (Fig. S4 and S5a, b†). The adsorption energy of MET on Zn(101) is −2.3562 eV, which is lower than those for Zn(002) and Zn(100), indicating the preferential adsorption. However, the presence of MET additives induces a weaker adsorption of Zn^{2+} on Zn(101) than the other two crystal planes, leading to a slower growth rate and the final dominant orientation of the Zn(101), according to the Bravais principle. Meanwhile, Zn^{2+} has the lowest desorption energy on the Zn(101) crystal plane, implying a faster dissolving capacity of Zn anodes on this plane (Fig.-S5c†). This further contributes to a much slower growth speed on Zn(101), considering one complete plating/stripping cycle, and thus gradually enhances the orientational intensity of Zn(101) with increasing numbers of cycles. These results can further be supported by the XRD data of the Zn stripping surface at different cycles (Fig. S6†). In addition, the regular terraced field morphology can also be found in the deposited surfaces of the Zn anode after 10 plating/stripping cycles in the Zn(ClO$_4$)$_2$–MET electrolyte, further demonstrating the modulating effect of MET molecules on the crystal surfaces (Fig. S7†). This special modulation on reversibly dominant Zn(101) is helpful for a long-term smooth deposition process on the Zn anodes, which can be observed *in situ* by optical microscopy (Fig. 1e, with a current density of 20 mA cm^{-2}). The homemade *in situ* optical micrograph system and detailed area of the device image are shown in Fig. S8.† As the deposition time increased, the Zn foil displayed significantly growing dendrites in pure Zn(ClO$_4$)$_2$ as well as obvious bubbles. In contrast, the Zn foil remained flat without any bubbles in the Zn(ClO$_4$)$_2$–MET electrolyte, revealing the significant function of MET in stabilizing the Zn anodes.
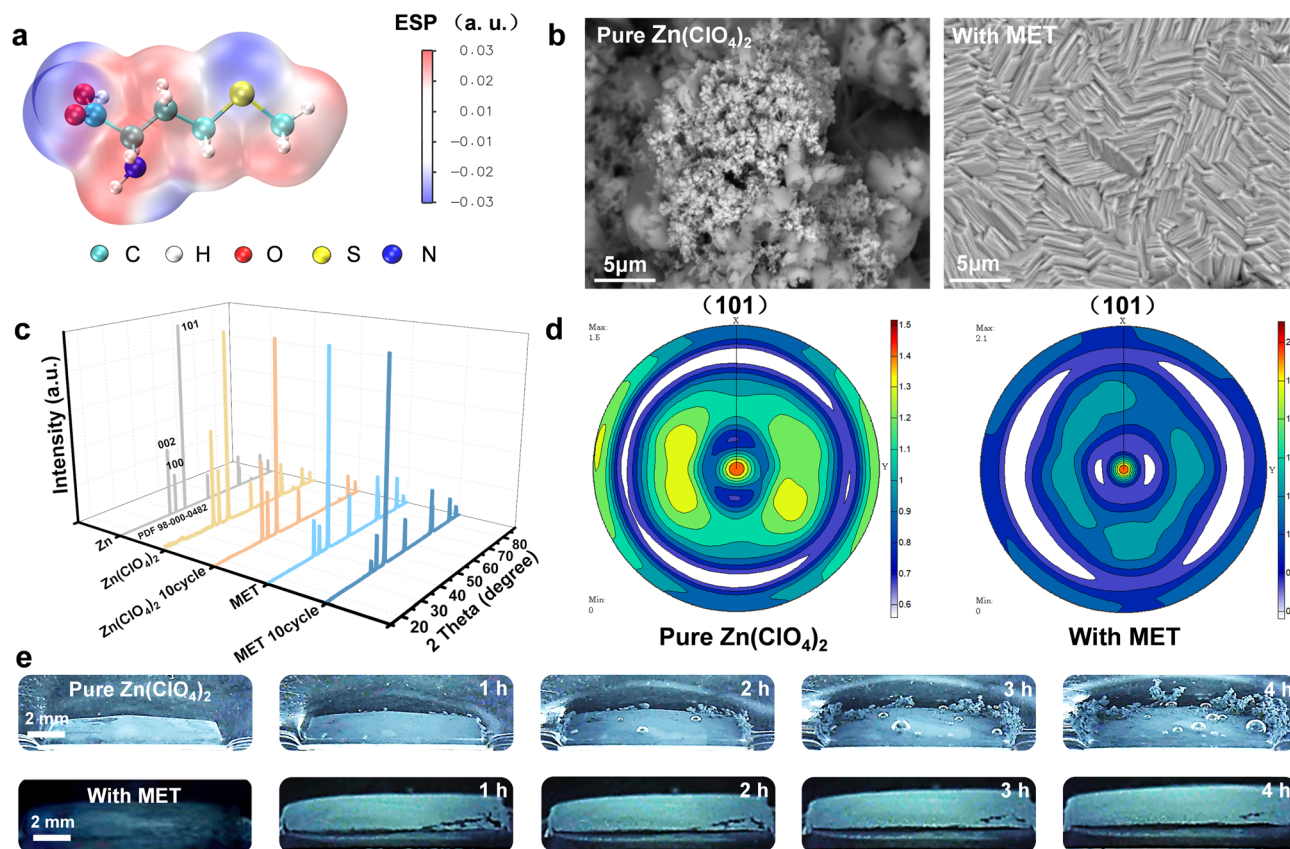
Fig. 1 Effect of MET additives on the surface of the Zn anode. (a) ESP of MET molecules; (b) SEM images of the Zn layer obtained from the plating electrolyte composed of different electrolytes at 10 mA cm^{-2} for 1 h; (c) XRD patterns of the Zn foil after several cycles in different electrolytes at 10 mA cm^{-2} and 10 mA h cm^{-2}; (d) Zn(101) pole figures of deposited Zn anodes under different electrolytes; (e) *in situ* optical micrographs recording the varying processes of Zn foil deposition in different electrolytes.

Adsorption of MET on the Zn anode and its modulation of the EEI

To study the adsorption behavior of the MET additive on the Zn anode surface, theoretical calculations and a series of experiments were conducted. Molecular dynamics (MD) simulations were first employed to trace the distribution of MET molecules around the Zn anode in the Zn(ClO$_4$)$_2$–MET electrolyte (Fig. 2a–c). The state of the MET molecule after the equilibrium process is shown in Fig. 2c. In this simulated model, the Zn anode was set in the center. By considering different distances away from the Zn anode, it can be inferred that peak 1 represents the number density of first-layer MET molecules closely adsorbed on the Zn anode surface (also called IHP) and peak 2 represents the number density of second-layer MET molecules in the OHP. Since our model is constructed in a symmetric style, peaks 3 and 4 represent the same parameters as peaks 1 and 2, respectively. Moreover, the Zn–N distance remained constant after stable adsorption (Fig. 2d), indicating the robust coordination function between the MET additive and Zn anode. Subsequently, the adsorption energies of MET, H$_2$O, and Zn atoms on the Zn anode were determined by DFT calculations. The MET molecule displayed the strongest adsorption energy, indicating its preferential adsorption on the Zn anode (Fig. 2e). Additionally, zeta potential measurements of the Zn anode soaked in different electrolyte systems

were collected, as presented in Fig. 2f. The presence of MET lowered the zeta potential from −111.4 mV to −260.5 mV, proving the effective adsorption of MET on the surface of the Zn anode.

The differential capacitance of the Zn(ClO$_4$)$_2$–MET electrolyte system decreases compared to that of the pure Zn(ClO$_4$)$_2$ system due to a smaller dielectric constant and larger volume of the MET molecule than that of H$_2$O molecule. Additionally, the MET molecule is adsorbed on the Zn anode through the –NH$_2$ group, leading to a positive shift of the potential of zero charge (PZC), as indicated in Fig. 2g. To further demonstrate the adsorption behaviour of MET on Zn anodes, X-ray electron spectroscopy (XPS) tests were performed. For pure MET powder, a peak located at 400.75 eV corresponding to –NH$_2$ can be observed (Fig. 2h, upper).[36,37] For the Zn foil immersed in the Zn(ClO$_4$)$_2$–MET electrolyte for 1 h, an obvious peak (Fig. 2h, bottom) can also be observed, but with a small shift to a lower binding energy (400.03 eV). Since there is no peak in the core level N spectrum for pure Zn foil (Fig. S9†), this should be ascribed to the formation of Zn–N bonds between MET molecules and the Zn foil.

Electrochemical performance of Zn anodes in different electrolytes and the corresponding mechanism

To further investigate the detailed function of MET additives, a series of electrochemical behaviors of the Zn anode in the
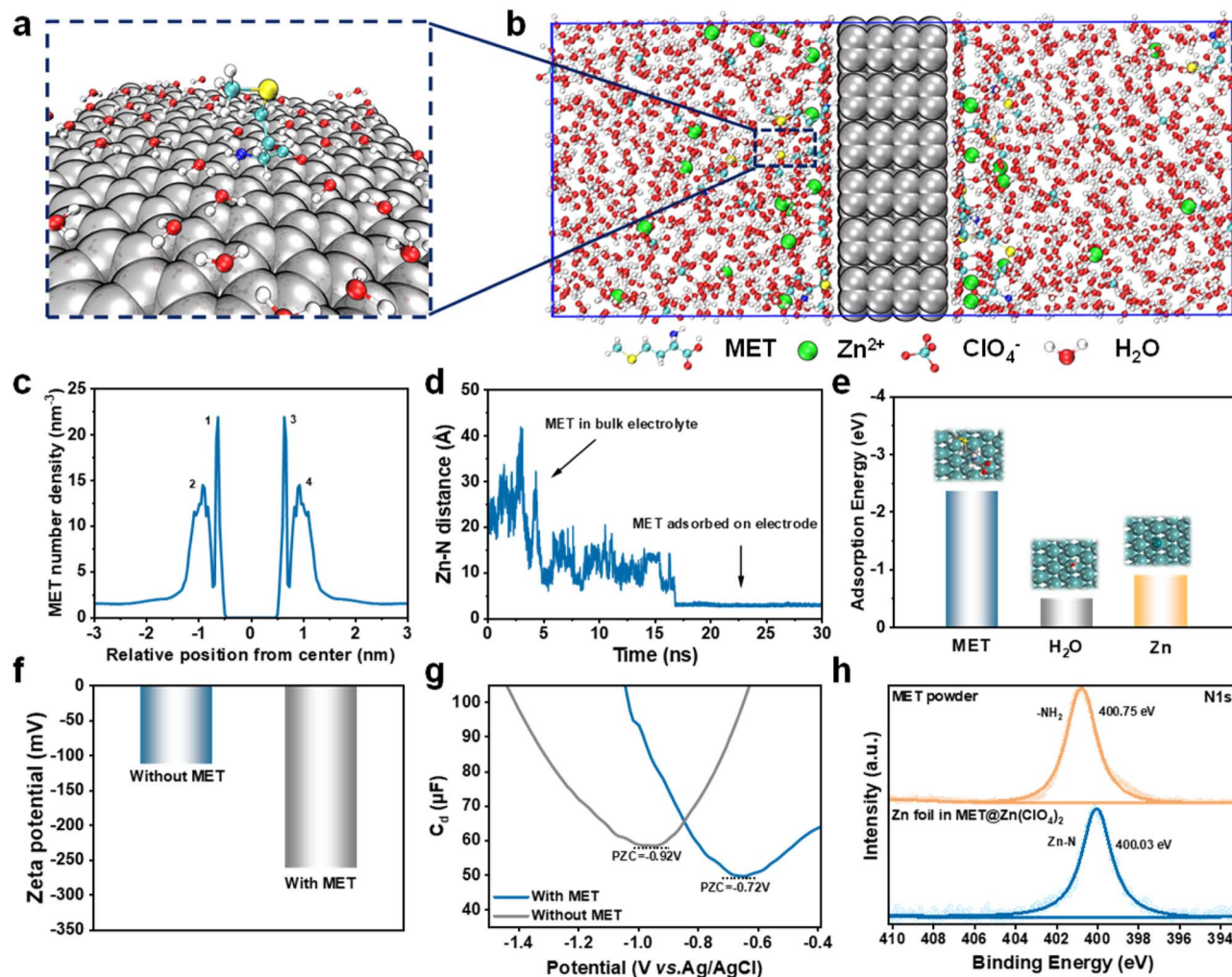
Fig. 2 (a) Theoretical calculations and characterization for the adsorption behavior of MET molecules on the Zn anodes. (b) Model presenting the MET additives adsorbed on the surface of the Zn anodes in the $Zn(ClO_4)_2$ electrolyte, (c) statistics of the MET molecular number density *versus* relative distance along the vertical direction upon setting the Zn anode at the central position, (d) temporal average distance between the Zn atoms on the surface of the anodes and N atoms from MET molecules derived from the MD simulations, (e) adsorption energy of the Zn atom, MET and H_2O molecules on the Zn anode, (f) zeta potentials of Zn anodes soaked in different electrolytes, (g) PZC curves of different electrolytes, and (h) XPS spectra of the core level N of MET powder and Zn foil after immersion in MET electrolyte.

$Zn(ClO_4)_2$–MET electrolyte, such as corrosive inhibition, Zn^{2+} diffusion and HER were studied. Cyclic voltammogram curves in the $Zn(ClO_4)_2$–MET electrolyte with a pair of redox peaks exhibit the reversible Zn plating/stripping processes in both electrolyte systems (Fig. S10†). As indicated in the linear polarization measurements of Fig. 3a, the introduction of MET results in a lower corrosion current of 0.51 mA cm^{-2} and corrosion potential of −0.919 V compared to those of the pure $Zn(ClO_4)_2$ system (0.68 mA cm^{-2} and −0.942 V, respectively). These indicate that the MET additive can limit the common side reactions during the reversible Zn plating/stripping procedures. In addition, the diffusion behavior of Zn^{2+} on the Zn anode was investigated by the chronoamperometry method, as demonstrated in Fig. 3b. Upon setting the overpotential to −150 mV, the current densities of the $Zn(ClO_4)_2$ system increase rapidly in the first 15 s, representing the rampant 2D diffusion of Zn^{2+} laterally along the surface to find the most favorable location for

charge transfer. In the following 600 s, the current density of the system continues to increase due to the subsequent 3D diffusion: the adsorbed Zn^{2+} gathers on a handful of nucleation sites to reduce and potentially induce the inhomogeneous Zn dendrite.[28] Conversely, the introduction of MET additives results in a much more stable current density, indicating a constrained 2D diffusion process as well as more controllable Zn^{2+} deposition behavior. It can be observed that the addition of MET results in an increase in the nucleation overpotential, which can effectively regulate the Zn^{2+} deposition speed (Fig. 3c). Subsequently, HER activity was investigated, as shown in Fig. 3d. Compared with pure $Zn(ClO_4)_2$, the introduced MET molecules increased the overpotential by 72 mV, indicating a remarkable effect in inhibiting HER. Moreover, the MET additive can also effectively limit oxygen evolution, increasing the overpotential by 69 mV compared with the pure $Zn(ClO_4)_2$ electrolyte (Fig. 3e). Therefore, the MET additive is capable of
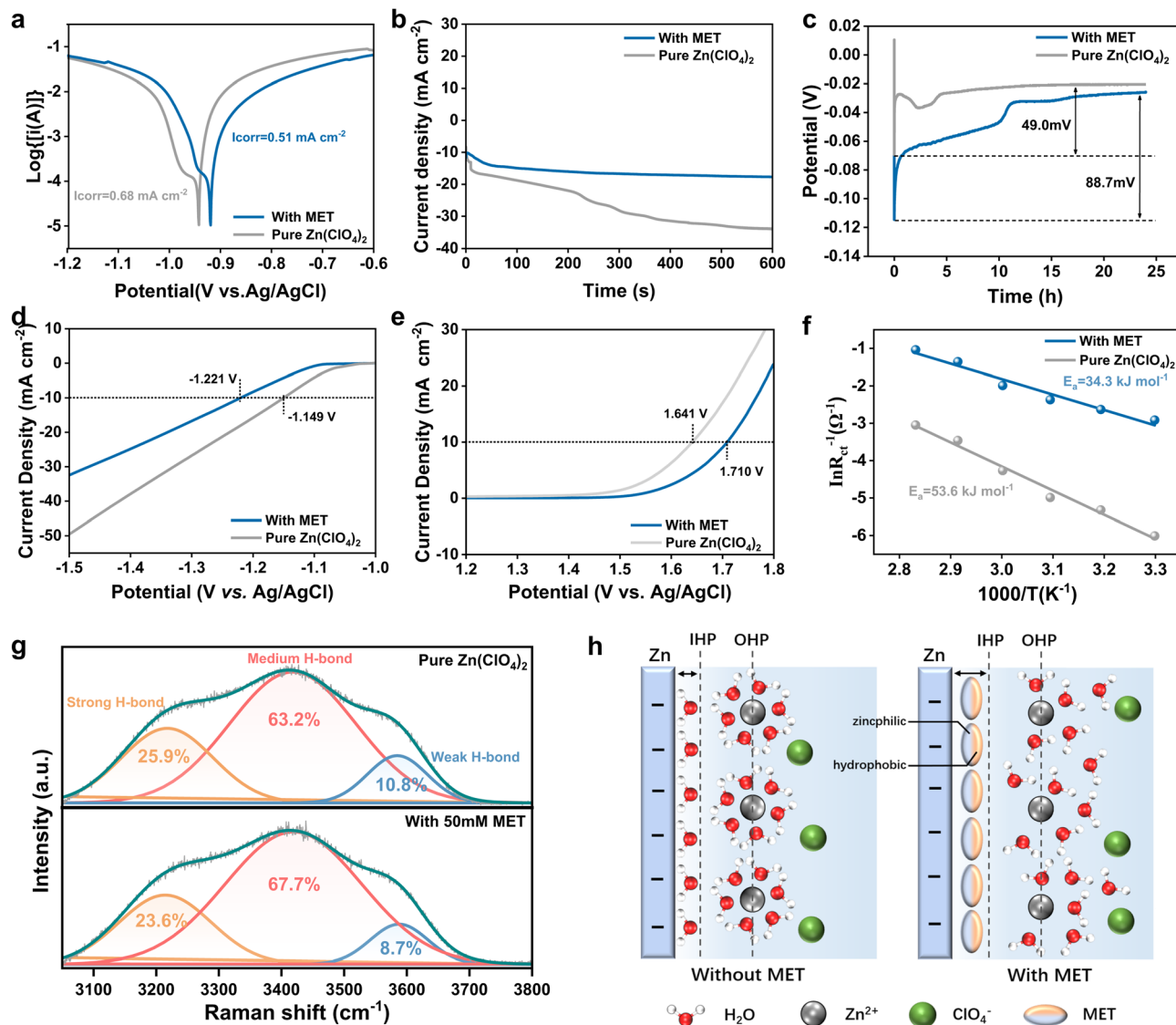
Fig. 3 Electrochemical measurements, spectra and schemes elucidating the regulating principle of MET to stabilize the Zn anode. (a) Tafel plot, (b) chronoamperometry curves, (c) nucleation overpotential and linear scanning curves indicating (d) hydrogen evolution, (e) oxygen evolution reactions, (f) desolvation energy and (g) Raman spectra of EEI in different electrolytes. (h) Schematic of adjusting function of MET for the EDL structure on Zn anodes.

broadening the decomposition window of H_2O molecules inside the electrolyte, ensuring better stability of the whole system. Finally, the role of the MET additives in the desolvation ability of Zn^{2+} was investigated using Nyquist plots of the symmetric cell at different temperatures (Fig. S11†). As shown in Fig. 3f, the desolvation energy of Zn^{2+} in pure $Zn(ClO_4)_2$ (53.6 kJ mol^{-1}) is higher than that in $Zn(ClO_4)_2$–MET (34.3 kJ mol^{-1}), indicating that the MET additive can reduce the Zn^{2+} desolvation barrier to obtain better dynamic performance.

To further investigate in detail the modulation by the MET additive of the water structure in bulk electrolyte and EEI, Raman measurements were performed. By varying the laser to focus on different heights of the electrolyte, different Raman spectra for different electrolyte environments were obtained. The results in Fig. S12, S13† and 3g were gathered in the EEI

region, indicating different O–H stretching modes of H_2O in the range of 3000–3800 cm^{-1} for electrolyte systems with and without MET additives.[38] The broadband in this region decreases upon increasing the MET concentration (Fig. S12†), while the characteristic peak of MET at 2926 cm^{-1} was also observed to be more pronounced at higher concentrations.[39,40] To better understand the specific water structure, different kinds of HB were analyzed using the above Raman spectra (Fig. 3g and S13†). The fitting spectra show that the O–H stretching band can be divided into three different components corresponding to different types of O–H stretching vibrations.[41,42] The low (orange), medium (pink) and high (blue) wavenumber components indicate strong, medium and weak hydrogen bonding interactions, respectively.[43,44] The addition of MET molecules resulted in a reduction of strong HB content of

23.6% at the EEI (compared to 25.9% for the pure $Zn(ClO_4)_2$ electrolyte). The above-mentioned analysis is consistent with the MD results (Fig. S14†), implying that the dense HB networks at the EEI were broken by the addition of MET molecules.

Therefore, the mechanism by which the MET additives improve the performance of the anodes is represented as in Fig. 3h. Commonly, the EDL is composed of the inner Helmholtz layer (IHP), with H_2O molecules adsorbed on the anode surface, and the outer Helmholtz layer (OHP), consisting of Zn^{2+} solvation structures. The MET additive introduced into the pure $Zn(ClO_4)_2$ electrolyte can perform the following three main functions. (1) Due to the zincophilic nature of the $-NH_2$ group, MET molecules will preferentially be adsorbed on the Zn anode surface, inducing Zn(101) crystal plane orientation and achieving a highly reversible flat Zn coating. (2) Because of the hydrophobicity of the $S-CH_3$ group, the desolvation process of Zn^{2+} acquires better kinetics, and MET molecules on the Zn anode surface can destroy HB networks at the EEI and inhibit the occurrence of side reactions. (3) When all these properties are combined, the MET additive can greatly modulate the stability of the Zn anodes.

The effective function of MET additives for stabilizing Zn anodes was then proved by comparing the cycling stability of different electrolytes in Zn//Zn symmetric cells. The suitable

concentration of MET was first investigated, as shown in Fig. S15.† Under the conditions of 10 mA cm^{-2}/10 mA h cm^{-2}, the cycle life of the symmetric cell continued to increase along with an increasing MET concentration up to 50 mM (318 h). Upon further increasing the MET concentration up to 75 mM, the polarization voltage increased significantly, resulting in a slightly decreased cycle life due to the restricted migration of Zn^{2+}. Therefore, the concentration of 50 mM was chosen for all the following experiments. Although the MET can result in a decrease in the pH value of the electrolyte system, this is not one of the critical factors affecting the performance of the Zn anodes, as revealed in Discussion S1 and Fig. S16.† As illustrated in Fig. 4a–c, the cycle lives of the symmetric cell in the pure $Zn(ClO_4)_2$ electrolyte are only 200 h and 25 h at 1 mA cm^{-2}/1 mA h cm^{-2} and 5 mA cm^{-2}/5 mA h cm^{-2}, respectively. Fast failure occurred at 10 mA cm^{-2}/10 mA h cm^{-2} (only 15 h) accompanied by a sudden increase in the polarization voltage. In sharp contrast, the cycle life of symmetric cells using the $Zn(ClO_4)_2$–MET electrolyte was much better, as long as 4500 h, 1165 h and 318 h under 1, 5 and 10 mA cm^{-2}/10 mA h cm^{-2}, respectively, confirming the great improvement effect on the stability of the anodes.

Depth of discharge (DOD) performance is an important parameter to evaluate the utilization efficiency of Zn anodes. Therefore, long cycle tests under 30% DOD conditions were
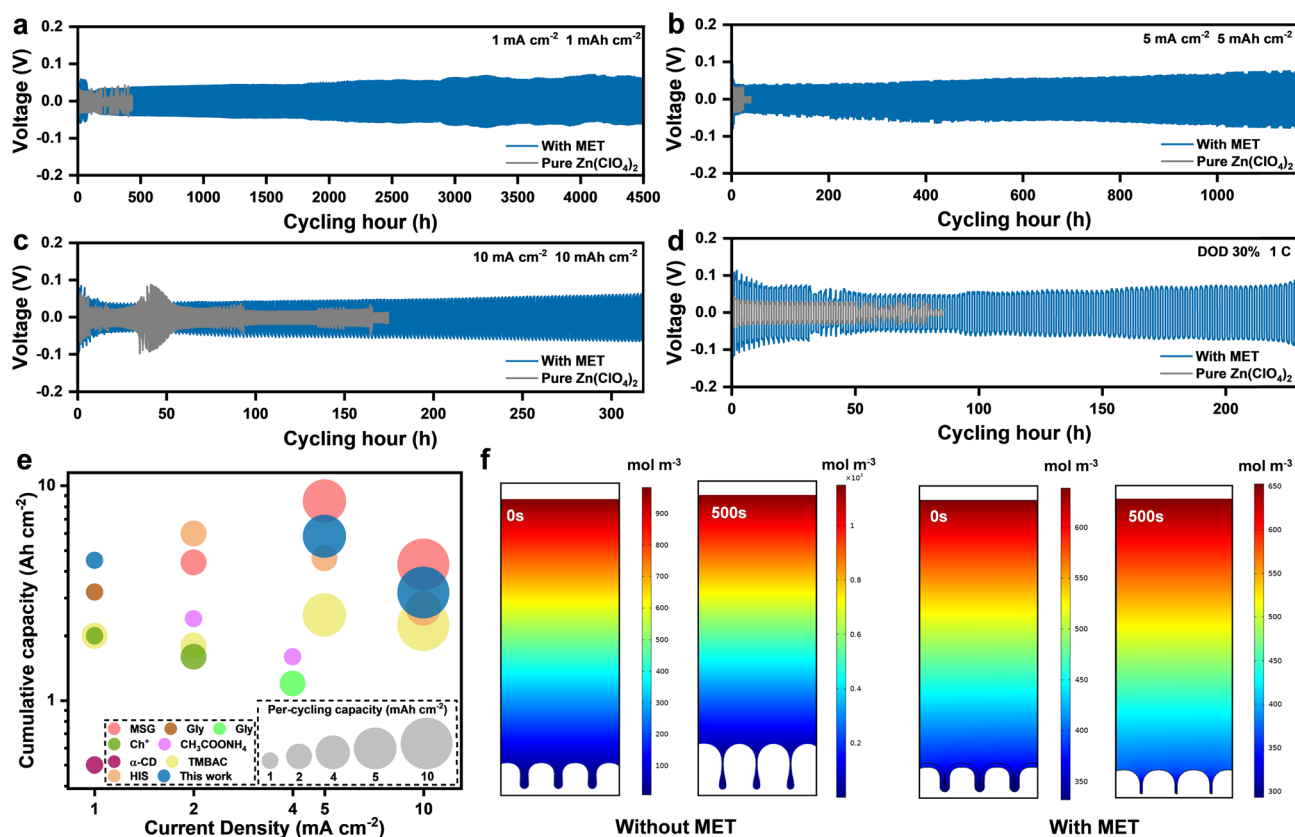

Fig. 4 Reversible Zn plating/stripping behaviors based on Zn//Zn cells and long-term cycling performance comparison of Zn//Zn symmetric cells under different current densities and areal capacities of (a) 1 mA cm^{-2}/1 mA h cm^{-2}, (b) 5 mA cm^{-2}/5 mA h cm^{-2}, (c) 10 mA cm^{-2}/10 mA h cm^{-2}, and (d) 30% DOD (20 μm Zn foil), in different electrolytes. (e) Comparison of key performance parameters of Zn//Zn symmetric cells from this work and previously reported work based on electrolyte additive strategies. (f) FEA of Zn dendrite growth and concentration gradients in different electrolytes (the white part is the Zn electrode).

performed for Zn//Zn symmetric cells (with thicker Zn of 20 μm) under different electrolytes, as shown in Fig. 4d. It can be observed that a stable cycle of over 230 hours can still be obtained with MET additives, which is much better than with the pure Zn(ClO₄)₂ system (about 50 hours). For overall comparison, the key parameters—including cumulative plated capacity, areal capacity per cycle and current density of this

work—and recently published studies using other additives are summarized in Table S2† and Fig. 4e.[29–32,45–48] Our work shows an excellent cycling stability in Zn//Zn symmetric cells, especially at higher current densities, compared with other studies with the same regulation type.

In addition, finite element analyses (FEA) were performed by simulating the plating/stripping process under different
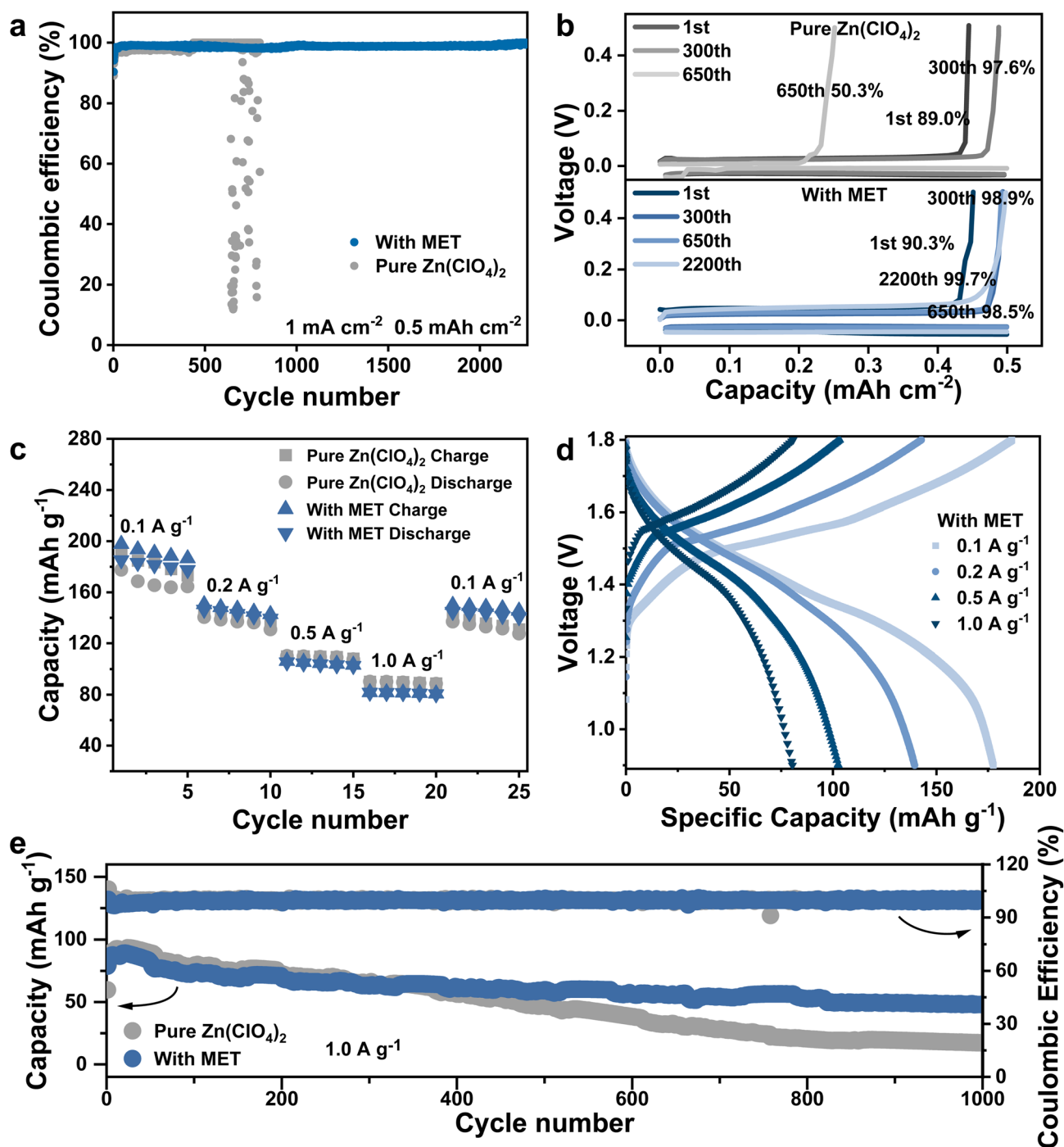

Fig. 5 Comparison of Zn//Cu asymmetric cell and Zn//MnO₂ full cell performance under different electrolyte systems. (a) CE measurements of Zn//Cu cells under different electrolyte systems; (b) the corresponding voltage profiles at various cycles; (c) rate performance at different current densities ranging from 0.1 to 1.0 A g⁻¹; (d) the corresponding charge–discharge curves of Zn–MnO₂ full cells under the Zn(ClO₄)₂–MET electrolyte; and (e) cycling stability at a current density of 1.0 A g⁻¹ under different electrolyte systems.

electrolyte systems. As exhibited in Fig. 4f, Zn^{2+} tends to be deposited continuously at the dendrites due to the tip effect in pure $Zn(ClO_4)_2$ and eventually intensifies the serious problem of uncontrolled dendrite growth. In contrast, the MET additive will be adsorbed on the Zn anode surface before dendrite growth, thus shielding the tip electric field and promoting continuous filling of nearby concave surfaces to flatten the deposited surface. Meanwhile, MET molecules can adjust the concentration gradient of the electrolyte and reduce the concentration polarization, guaranteeing enough Zn^{2+} in the EEI for continuous deposition.

Performance of Zn//Cu cells and Zn//MnO$_2$ full cells

To verify the excellent functionality of MET additives in practical devices, Zn//Cu cells and Zn//MnO$_2$ full cells were prepared using different electrolytes. Cyclic plating/stripping tests were performed in Zn//Cu cells to evaluate the reversible conversion efficiency between Zn/Zn^{2+}, as demonstrated in Fig. 5a and b. Clearly, in the first few cycles of different electrolyte systems, the deposition/dissolution processes of Zn on Cu foil encounter a lattice fitting stage (or reshaped Zn coordination), thus the coulombic efficiency (CE) is rather low.[49] Upon setting the test conditions to 1 mA cm^{-2}/0.5 mA h cm^{-2} in the pure $Zn(ClO_4)_2$ electrolyte, the Zn//Cu cell remained stable for the initial 640 cycles. After that, the device encountered unstable cycling with a low CE. It is noteworthy that the $Zn(ClO_4)_2$–MET electrolyte system can maintain stable cycling for over 2200 cycles under the same test conditions and realize a high average CE of 98.9% (50–2200 cycles).

Finally, using different electrolytes, Zn//MnO$_2$ full cells were compared. There was no significant difference in the overall rate performances (Fig. 5c) with or without MET additives (Fig. 5d and S17†), indicating that MET additives rarely influence the specific capacities. Then, reversible charge/discharge cycles were performed at a current density of 1 A g^{-1} to examine the long-term stability performance, as shown in Fig. 5e. For the pure $Zn(ClO_4)_2$ electrolyte system, the capacity decreased from 59.7 mA h g^{-1} to 17.2 mA h g^{-1} after 1000 cycles, with a capacity retention of only 28.8%. In contrast, full cells using the $Zn(ClO_4)_2$–MET electrolyte can achieve a much higher capacity retention of 79.9% after 1000 cycles. The above results imply that the MET additive can improve the CE of reversible Zn plating/stripping and long-term stability of AZIB full cells.

Conclusions

In summary, we propose the methionine (MET) molecule as an additive for aqueous electrolytes to achieve stable Zn anodes. Combining theoretical calculations, molecular dynamics simulations, crystallographic characterization, and electrochemical characterizations, the modulating mechanism of the MET additive on the Zn anode stability can be obtained. First, MET molecules can be preferentially adsorbed on the Zn anode to change the electric double layer structure and disrupt the hydrogen bonding network among H$_2$O molecules at the electrode/electrolyte interface (EEI), inhibiting the occurrence

of various side reactions. At the same time, there is also a crystal surface modulation effect, which facilies the preferential domination by the Zn(101) crystal plane, and can effectively inhibit the dendrite growth due to the highly reversible plating/stripping behaviours. As validated, the MET additive can result in excellent cycling performance of the Zn//Zn symmetric cell, achieving 4500 h, 1165 h and 318 h under the conditions of 1 mA cm^{-2}/1 mA h cm^{-2}, 5 mA cm^{-2}/5 mA h cm^{-2}, and 10 mA cm^{-2}/10 mA h cm^{-2}, respectively. It is noteworthy that a stable cycling of more than 2200 cycles can also be achieved in Zn//Cu asymmetric cells with the assistance of MET additives, with an average coulombic efficiency of up to 98.9%. In addition, the Zn//MnO$_2$ full cell using the $Zn(ClO_4)_2$–MET electrolyte also demonstrates an excellent cycling stability, with a capacity retention of 79.9% after 1000 cycles. All of the above indicates that MET additives can be excellent candidates for improving the stability of Zn anodes and AZIBs, which can potentially contribute to the fast development of various aqueous batteries using metals as anodes.

Data availability

Data are available upon request from the authors.

Author contributions

Conceptualization: Y. X. L., M. J. Q., P. S., W. J. M.; data curation: Y. X. L., M. J. Q.; formal analysis: Y. X. L., M. J. Q.; funding acquisition: P. S., W. J. M.; software: M. J. Q., P. S.; supervision: P. S., W. J. M.; visualization: Y. X. L., M. J. Q.; writing-original draft: Y. X. L., M. J. Q.; writing-review & editing: P. S., W. J. M.

Conflicts of interest

There are no conflicts to declare.

Acknowledgements

References

1 B. Obama, The irreversible momentum of clean energy, *Science*, 2017, **355**, 126–129.

2 Q. Li, Y. Zhao, F. Mo, D. Wang, Q. Yang, Z. Huang, G. Liang, A. Chen and C. Zhi, Dendrites issues and advances in Zn anode for aqueous rechargeable Zn-based batteries, *EcoMat*, 2020, **2**, e12035.

3 H. Pan, Y. Shao, P. Yan, Y. Cheng, K. S. Han, Z. Nie, C. Wang, J. Yang, X. Li, P. Bhattacharya, K. T. Mueller and J. Liu, Reversible aqueous zinc/manganese oxide energy storage from conversion reactions, *Nat. Energy*, 2016, **1**, 16039.

4 N. Chen, M. Qiu, C. Zhao, G. Yan, W. Mai and P. Sun, Monitoring the Zn ion storage of Prussian blue analog via in situ spectral imaging strategy, *Appl. Phys. Lett.*, 2023, **122**, 263905.

5 P. Ruan, S. Liang, B. Lu, H. J. Fan and J. Zhou, Design Strategies for High-Energy-Density Aqueous Zinc Batteries, *Angew. Chem., Int. Ed.*, 2022, **61**, e202200598.

6 D. Chao, W. Zhou, F. Xie, C. Ye, H. Li, M. Jaroniec and S. Z. Qiao, Roadmap for advanced aqueous batteries: from design of materials to applications, *Sci. Adv.*, 2020, **6**, eaba4098.

7 C. Li, X. Xie, S. Liang and J. Zhou, Issues and Future Perspective on Zinc Metal Anode for Rechargeable Aqueous Zinc-ion Batteries, *Energy Environ. Mater.*, 2020, **3**, 146–159.

8 R. Qin, Y. Wang, L. Yao, L. Yang, Q. Zhao, S. Ding, L. Liu and F. Pan, Progress in interface structure and modification of zinc anode for aqueous batteries, *Nano Energy*, 2022, **98**, 107333.

9 M. Zhou, Y. Chen, G. Fang and S. Liang, Electrolyte/electrode interfacial electrochemical behaviors and optimization strategies in aqueous zinc-ion batteries, *Energy Storage Mater.*, 2022, **45**, 618–646.

10 A. Chen, C. Zhao, J. Gao, Z. Guo, X. Lu, J. Zhang, Z. Liu, M. Wang, N. Liu, L. Fan, Y. Zhang and N. Zhang, Multifunctional SEI-like structure coating stabilizing Zn anode at large current and capacity, *Energy Environ. Sci.*, 2023, **16**, 275–284.

11 G. Li, X. Wang, S. Lv, J. Wang, W. Yu, X. Dong and D. Liu, In Situ Constructing a Film-Coated 3D Porous Zn Anode by Iodine Etching Strategy Toward Horizontally Arranged Dendrite-Free Zn Deposition, *Adv. Funct. Mater.*, 2022, **33**, 2208288.

12 W. Li, Q. Zhang, Z. Yang, H. Ji, T. Wu, H. Wang, Z. Cai, C. Xie, Y. Li and H. Wang, Isotropic Amorphous Protective Layer with Uniform Interfacial Zincophobicity for Stable Zinc Anode, *Small*, 2022, **18**, 2205667.

13 H. Yang, Z. Chang, Y. Qiao, H. Deng, X. Mu, P. He and H. Zhou, Constructing a Super-Saturated Electrolyte Front Surface for Stable Rechargeable Aqueous Zinc Batteries, *Angew. Chem., Int. Ed. Engl.*, 2020, **59**, 9377–9381.

14 M. Zhu, Q. Ran, H. Huang, Y. Xie, M. Zhong, G. Lu, F.-Q. Bai, X.-Y. Lang, X. Jia and D. Chao, Interface Reversible Electric Field Regulated by Amphoteric Charged Protein-Based Coating toward High-Rate and Robust Zn Anode, *Nano-Micro Lett.*, 2022, **14**, 219.

15 S. Xie, Y. Li and L. Dong, Stable anode-free zinc-ion batteries enabled by alloy network-modulated zinc deposition interface, *J. Energy Chem.*, 2023, **76**, 32–40.

16 J. L. Yang, J. Li, J. W. Zhao, K. Liu, P. Yang and H. J. Fan, Stable Zinc Anodes Enabled by a Zincophilic Polyanionic Hydrogel Layer, *Adv. Mater.*, 2022, **34**, e2202382.

17 A. Bayaguud, X. Luo, Y. Fu and C. Zhu, Cationic Surfactant-Type Electrolyte Additive Enables Three-Dimensional Dendrite-Free Zinc Anode for Stable Zinc-Ion Batteries, *ACS Energy Lett.*, 2020, **5**, 3012–3020.

18 H. Qiu, X. Du, J. Zhao, Y. Wang, J. Ju, Z. Chen, Z. Hu, D. Yan, X. Zhou and G. Cui, Zinc anode-compatible in-situ solid electrolyte interphase via cation solvation modulation, *Nat. Commun.*, 2019, **10**, 5374.

19 X. Zeng, J. Mao, J. Hao, J. Liu, S. Liu, Z. Wang, Y. Wang, S. Zhang, T. Zheng, J. Liu, P. Rao and Z. Guo, Electrolyte Design for In Situ Construction of Highly Zn^{2+}-Conductive Solid Electrolyte Interface to Enable High-Performance Aqueous Zn-Ion Batteries under Practical Conditions, *Adv. Mater.*, 2021, **33**, e2007416.

20 S. J. Zhang, J. Hao, D. Luo, P. F. Zhang, B. Zhang, K. Davey, Z. Lin and S. Z. Qiao, Dual-Function Electrolyte Additive for Highly Reversible Zn Anode, *Adv. Energy Mater.*, 2021, **11**, 2102010.

21 Y. Xu, J. Zhu, J. Feng, Y. Wang, X. Wu, P. Ma, X. Zhang, G. Wang and X. Yan, A rechargeable aqueous zinc/sodium manganese oxides battery with robust performance enabled by Na_2SO_4 electrolyte additive, *Energy Storage Mater.*, 2021, **38**, 299–308.

22 Y. Li, P. Wu, W. Zhong, C. Xie, Y. Xie, Q. Zhang, D. Sun, Y. Tang and H. Wang, A progressive nucleation mechanism enables stable zinc stripping–plating behavior, *Energy Environ. Sci.*, 2021, **14**, 5563–5571.

23 M. Song and C.-L. Zhong, Achieving both high reversible and stable Zn anode by a practical glucose electrolyte additive toward high-performance Zn-ion batteries, *Rare Met.*, 2021, **41**, 356–360.

24 C.-X. Xu and J.-J. Jiang, Electrolytes speed up development of zinc batteries, *Rare Met.*, 2021, **40**, 749–751.

25 M. Qiu, L. Ma, P. Sun, Z. Wang, G. Cui and W. Mai, Manipulating Interfacial Stability Via Absorption-Competition Mechanism for Long-Lifespan Zn Anode, *Nano-Micro Lett.*, 2021, **14**, 31.

26 M. Qiu, P. Sun, A. Qin, G. Cui and W. Mai, Metal-coordination chemistry guiding preferred crystallographic orientation for reversible zinc anode, *Energy Storage Mater.*, 2022, **49**, 463–470.

27 M. Qiu, P. Sun, Y. Wang, L. Ma, C. Zhi and W. Mai, Anion-Trap Engineering toward Remarkable Crystallographic Reorientation and Efficient Cation Migration of Zn Ion Batteries, *Angew. Chem., Int. Ed. Engl.*, 2022, **61**, e202210979.

28 M. Zhou, S. Guo, J. Li, X. Luo, Z. Liu, T. Zhang, X. Cao, M. Long, B. Lu, A. Pan, G. Fang, J. Zhou and S. Liang, Surface-Preferred Crystal Plane for a Stable and Reversible Zinc Anode, *Adv. Mater.*, 2021, **33**, e2100187.

29 K. Zhao, G. Fan, J. Liu, F. Liu, J. Li, X. Zhou, Y. Ni, M. Yu, Y. M. Zhang, H. Su, Q. Liu and F. Cheng, Boosting the Kinetics and Stability of Zn Anodes in Aqueous Electrolytes with Supramolecular Cyclodextrin Additives, *J. Am. Chem. Soc.*, 2022, **144**, 11129–11137.

30 C. Lin, X. Yang, P. Xiong, H. Lin, L. He, Q. Yao, M. Wei, Q. Qian, Q. Chen and L. Zeng, High-Rate, Large Capacity, and Long Life Dendrite-Free Zn Metal Anode Enabled by Trifunctional Electrolyte Additive with a Wide Temperature Range, *Adv. Sci.*, 2022, **9**, e2201433.

31 X. Nie, L. Miao, W. Yuan, G. Ma, S. Di, Y. Wang, S. Shen and N. Zhang, Cholinium Cations Enable Highly Compact and Dendrite-Free Zn Metal Anodes in Aqueous Electrolytes, *Adv. Funct. Mater.*, 2022, **32**, 2203905.

32 K. Guan, L. Tao, R. Yang, H. Zhang, N. Wang, H. Wan, J. Cui, J. Zhang, H. Wang and H. Wang, Anti-Corrosion for Reversible Zinc Anode via a Hydrophobic Interface in Aqueous Zinc Batteries, *Adv. Energy Mater.*, 2022, **12**, 2103557.

33 J. Cui, X. Liu, Y. Xie, K. Wu, Y. Wang, Y. Liu, J. Zhang, J. Yi and Y. Xia, Improved electrochemical reversibility of Zn plating/stripping: a promising approach to suppress water-induced issues through the formation of H-bonding, *Mater. Today Energy*, 2020, **18**, 100563.

34 H. Zhang, Y. Zhong, J. Li, Y. Liao, J. Zeng, Y. Shen, L. Yuan, Z. Li and Y. Huang, Inducing the Preferential Growth of Zn (002) Plane for Long Cycle Aqueous Zn-Ion Batteries, *Adv. Energy Mater.*, 2022, **13**, 2203254.

35 Y. Liang, M. Qiu, P. Sun and W. Mai, Comprehensive Review of Electrolyte Modification Strategies for Stabilizing Zn Metal Anodes, *Adv. Funct. Mater.*, 2023, **33**, 2304878.

36 R. A. Brizzolara, Methionine by X-ray Photoelectron Spectroscopy, *Surf. Sci. Spectra*, 1996, **4**, 96–101.

37 A. Artemenko, A. Shchukarev, P. Štenclová, T. Wågberg, J. Segervald, X. Jia and A. Kromka, Reference XPS spectra of amino acids, *IOP Conf. Ser.: Mater. Sci. Eng.*, 2021, **1050**, 012001.

38 J. G. Davis, K. P. Gierszal, P. Wang and D. Ben-Amotz, Water structural transformation at molecular hydrophobic interfaces, *Nature*, 2012, **491**, 582–585.

39 J. A. Lima, P. T. C. Freire, F. E. A. Melo, J. M. Filho, J. Fischer, R. W. A. Havenith, R. Broer and H. N. Bordallo, Using Raman spectroscopy to understand the origin of the phase transition observed in the crystalline sulfur based amino acid l-methionine, *Vib. Spectrosc.*, 2013, **65**, 132–141.

40 J. A. Lima, P. T. C. Freire, F. E. A. Melo, V. Lemos, J. Mendes Filho and P. S. Pizani, High pressure Raman spectra of L-methionine crystal, *J. Raman Spectrosc.*, 2008, **39**, 1356–1363.

41 H.-C. Chen, B.-J. Hwang, F.-D. Mai, Y.-C. Liu, C.-M. Lin, H.-S. Kuo, D.-S. Chou, M.-J. Lee, K.-H. Yang, C.-C. Yu, J.-R. Chen, T.-Y. Lo, H.-Y. Tsai, C.-P. Yang, C. Wang, H.-T. Hsieh and J. Rick, Active and Stable Liquid Water Innovatively Prepared Using Resonantly Illuminated Gold Nanoparticles, *ACS Nano*, 2014, **8**, 2704–2713.

42 L. F. Scatena, M. G. Brown and G. L. Richmond, Water at Hydrophobic Surfaces: Weak Hydrogen Bonding and Strong Orientation Effects, *Science*, 2001, **292**, 908–912.

43 M. Qiu, P. Sun, K. Han, Z. Pang, J. Du, J. Li, J. Chen, Z. L. Wang and W. Mai, Tailoring water structure with high-tetrahedral-entropy for antifreezing electrolytes and energy storage at -80 degrees C, *Nat. Commun.*, 2023, **14**, 601.

44 Y. H. Wang, S. Zheng, W. M. Yang, R. Y. Zhou, Q. F. He, P. Radjenovic, J. C. Dong, S. Li, J. Zheng, Z. L. Yang, G. Attard, F. Pan, Z. Q. Tian and J. F. Li, In situ Raman spectroscopy reveals the structure and dissociation of interfacial water, *Nature*, 2021, **600**, 81–85.

45 Y. Zhong, Z. Cheng, H. Zhang, J. Li, D. Liu, Y. Liao, J. Meng, Y. Shen and Y. Huang, Monosodium glutamate, an effective electrolyte additive to enhance cycling performance of Zn anode in aqueous battery, *Nano Energy*, 2022, **98**, 107220.

46 Z. Zhao, P. Li, Z. Zhang, H. Zhang and G. Li, Dendrite-free zinc anode enabled by Buffer-like additive via strong cationic specific absorption, *Chem. Eng. J.*, 2023, **454**, 140435.

47 Y. Liu, Y. An, L. Wu, J. Sun, F. Xiong, H. Tang, S. Chen, Y. Guo, L. Zhang, Q. An and L. Mai, Interfacial Chemistry Modulation via Amphoteric Glycine for a Highly Reversible Zinc Anode, *ACS Nano*, 2022, **17**, 552–560.

48 Q. Gou, H. Luo, Q. Zhang, J. Deng, R. Zhao, O. Odunmbaku, L. Wang, L. Li, Y. Zheng, J. Li, D. Chao and M. Li, Electrolyte Regulation of Bio-Inspired Zincophilic Additive toward High-Performance Dendrite-Free Aqueous Zinc-Ion Batteries, *Small*, 2023, **19**, e2207502.

49 P. Sun, L. Ma, W. Zhou, M. Qiu, Z. Wang, D. Chao and W. Mai, Simultaneous Regulation on Solvation Shell and Electrode Interface for Dendrite-Free Zn Ion Batteries Achieved by a Low-Cost Glucose Additive, *Angew. Chem., Int. Ed.*, 2021, **60**, 18247–18255.